Title

Noninvasive assessment of skin structure by combined photothermal radiometry and optical spectroscopy: coregistration with multiphoton microscopy.

Journal

Applied Optics, 57(18)

ISSN

1559-128X

Authors

Verdel, Nina
Lentsch, Griffin
Balu, Mihaela
et al.

Publication Date

2018-06-20

DOI

10.1364/ao.57.00d117

Peer reviewed

Research Article Vol. 57, No. 18 / 20 June 2018 / Applied Optics D117

applied optics

Noninvasive assessment of skin structure by combined photothermal radiometry and optical spectroscopy: coregistration with multiphoton microscopy

Nina Verdel,[1] Griffin Lentsch,[2] Mihaela Balu,[2] Bruce J. Tromberg,[2] and Boris Majaron[1,3,*]

[1]Jožef Stefan Institute, Department of Complex Matter, Jamova 39, 1000 Ljubljana, Slovenia
[2]Beckman Laser Institute, University of California, 1002 Health Sciences Rd., Irvine, California 92617, USA
[3]Faculty of Mathematics and Physics, University of Ljubljana, Jadranska 19, 1000 Ljubljana, Slovenia
*Corresponding author: boris.majaron@ijs.si

Received 18 January 2018; revised 19 March 2018; accepted 20 March 2018; posted 21 March 2018 (Doc. ID 319887); published 19 April 2018

We are combining two optical techniques, pulsed photothermal radiometry (PPTR) and diffuse reflectance spectroscopy (DRS), for noninvasive assessment of the structure and composition of human skin *in vivo*. The analysis involves simultaneous multidimensional fitting of the measured PPTR signals and DRS spectra with predictions of a numerical model of light transport (Monte Carlo) in a four-layer model optical model of human skin, accounting for the epidermis, papillary and reticular dermis, and subcutis. The assessed epidermal thickness values were tested by coregistration with a multiphoton microscope, which provides vertical sectioning capability based on two-photon excited fluorescence and second-harmonic generation in selected skin components. The comparison shows that these values correspond well to the maximal epidermal thicknesses measured in the multiphoton microscopy images, the rete ridges.

OCIS codes: (170.6510) Spectroscopy, tissue diagnostics; (170.6935) Tissue characterization; (180.2520) Fluorescence microscopy; (190.4180) Multiphoton processes; (290.6815) Thermal emission; (350.5340) Photothermal effects.

https://doi.org/10.1364/AO.57.00D117

1. INTRODUCTION

Pulsed photothermal radiometry (PPTR) involves measurements of transient dynamics in mid-infrared (IR) emission from a sample surface after exposure to a single light pulse. Beside the assessment of optical or thermal properties of homogeneous samples, light-induced temperature depth profiles can also be determined from such radiometric signals [1–3].

Quantitative assessment of structural properties and composition of multilayered tissue structures, such as human skin, however, requires solving an additional inverse problem of light transport in a scattering-dominated medium. This process relies on several assumptions, such as the scattering properties of the tissue layers, which may, however, vary with anatomical location, a person's age, gender, lifestyle (smoking), etc.

Because we found that the described approach does not allow for unique extraction of the relevant skin characteristics [4], we have decided to combine PPTR analysis with another optical technique, diffuse reflectance spectroscopy (DRS) in the visible spectral range. In a dedicated simulation study, we demonstrated that such a dual-modality approach significantly improves the robustness of the involved inverse analysis [5]. Namely, while PPTR is highly sensitive to depth distribution of selected absorbers, DRS employs spectral differentiation between different chromophores, characteristic for specific layers of human skin (e.g., melanin in the epidermis, oxyhemoglobin and deoxyhemoglobin in dermis, and subcutaneous adipose tissue).

We have thus far performed only provisional testing of such a dual-modality approach by comparing the assessed values for healthy skin with data in the literature [6,7] and analyzing their changes in response to external influences such as application of a blood-pressure cuff [8] or sun tanning. Based on encouraging results, we are tentatively applying the same approach in ongoing studies of hemodynamics in self-healing bruises [9] and the effects of aesthetic laser treatments [10], which represent further tests of its viability.

Admittedly, comparisons of our own results with the literature data are often inconclusive due to differences in included populations or other potentially relevant protocol details. Moreover, such testing is not sufficiently critical because the analyzed skin properties can vary a great deal in the human population and even within each person (both with anatomical

region and over time). For example, a dedicated study of epidermal thickness (ET) using the gold-standard cryo-histology approach [11] reported a mean ET for dorsal arm of 75 ± 13 μm. The same study also demonstrated, however, that the influence of anatomical site far exceeds interpersonal variations.

In the following, we thus present an objective, albeit only partial test of our dual-modality characterization of human skin *in vivo*, performed by coregistration with a multiphoton microscopy (MPM) system that provides optical sectioning capability [12,13]. By employing the contrast between two-photon excited fluorescence (TPEF) from biomolecules residing primarily in the epidermis and second-harmonic generation (SHG) in collagen fibers (present exclusively in the dermis), the ET can be easily assessed from the MPM cross-sectional images and compared with the values obtained from analysis of the same test sites based on combined PPTR and DRS.

2. METHODS

Two test sites were selected and marked on the dorsal (flexor) side of the forearm and upper arm, respectively, in a consenting volunteer (coauthor BM, male, age 54) with healthy skin of fair complexion (Fitzpatrick type II). The protocol for noninvasive characterization utilizing PPTR and DRS was approved by the Medical Ethics Committee of the Republic of Slovenia.

A. PPTR

Before the measurement, the test sites were tape-stripped to remove the superficial layer of desiccated epidermal cells (stratum corneum) [2,4]. This should ensure unimpaired heat diffusion all the way to the skin surface.

The test sites were irradiated with individual 1 ms light pulses at $\lambda = 532$ nm, emitted from a medical-grade laser (DualisVP by Fotona, Ljubljana, Slovenia). At the effective spot diameter of ~5 mm, the radiant exposure was approximately 0.30 J/cm^2. Radiative emission from the tissue surface was recorded using a fast mid-IR camera sensitive in the 3.5–5.1 μm wavelength range (SC7500 by FLIR Systems Inc.; see Fig. 1), at a rate of 1000 frames per second (Fig. 2).

One-dimensional PPTR signals were obtained from the acquired radiometric record by lateral averaging over a suitable area of interest (typically 1 mm × 1 mm) and subtracting the baseline value. The manufacturer-provided calibration system (Hypercal) was used for conversion of raw signal values to a radiometric temperature scale [3,4].

B. DRS

DRS spectra in the visible spectral range ($\lambda = 400$–700 nm) were measured using an integrating sphere with an internal light source (ISP-REF by Ocean Optics, Dunedin, Florida) and a fiber-connected compact optical spectrometer (USB4000, Ocean Optics) [4,14]. Prior to analysis, the common measurement artifact called single-beam substitution error was removed from each acquired DRS using an algebraic correction, developed earlier based both on theoretical analysis and experimental verification [14].

C. Model-Based Inverse Analysis

The structure and composition of the selected test site are assessed by simultaneously fitting the measured PPTR signals and

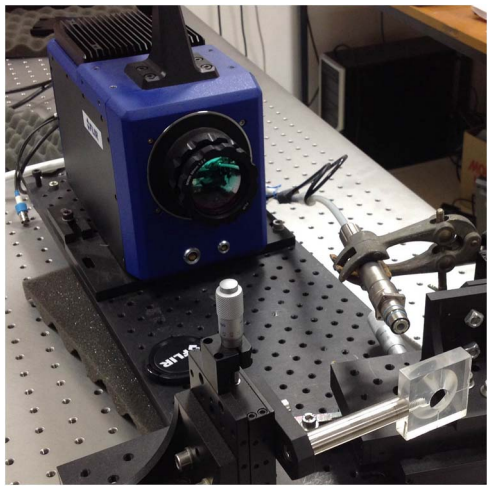

Fig. 1. Experimental setup for PPTR measurements, consisting of a fast mid-IR camera with a 50 mm objective, optical fiber for delivery of light pulses from a 532 nm laser, beam-shaping optics, and an aperture for accurate positioning of the selected test site.

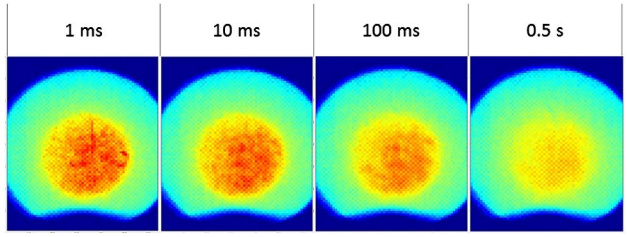

Fig. 2. Typical mid-IR images of a skin test site at different time delays after pulsed laser irradiation (indicated above each frame). The colors indicate radiometric temperatures, from 30°C (deep blue) to 35°C (red). The lateral dimension of each frame is 10 mm.

DRS spectra with corresponding predictions from a dedicated numerical model of light and heat transport in human skin. This is performed by objective multidimensional minimization of the residual norm using the nonlinear least-squares algorithm implemented as a function lsqnonlin in the MATLAB Optimization Toolbox (Mathworks Inc., Natick, Massachusetts).

The applied optical model of skin assumes four optically homogeneous layers, representing the epidermis, papillary and reticular dermis, and subcutis (adipose). The expressions that link the absorption properties of each skin layer and the fractional contents of the primary absorbers were reported earlier [4,15]. For example, the epidermal absorption coefficient, $\mu_{a,epi}$, is calculated using the relations [16]

$$\mu_{a,epi} = m\mu_{a,mel} + (1 - m)\mu_{a,base}, \quad (1)$$

$$\mu_{a,mel} = 6.6 \times 10^{10}\ \text{mm}^{-1}\left(\frac{\lambda}{\text{nm}}\right)^{-3.33}, \quad (2)$$

$$\mu_{a,base} = 0.0244\ \text{mm}^{-1} + 8.53\ \text{mm}^{-1}\exp\left(-\frac{\lambda - 154\ \text{nm}}{66.2\ \text{nm}}\right), \quad (3)$$

where $\mu_{a,mel}$ represents the melanin absorption spectrum and $\mu_{a,base}$ is the baseline absorption of bloodless skin.

The absorption coefficients for the papillary and reticular dermis are obtained in a manner analogous to Eq. (1), but of course considering the (mutually independent) fractional blood contents and oxygen saturation levels, and using the absorption spectra for fully oxygenated and deoxygenated whole blood, respectively [17].

In addition to the chromophore contents and thicknesses of the constitutive layers, we also optimize scattering properties of skin, according to the customary ansatz:

$$\mu_s'(\lambda) = a\left(\frac{\lambda}{500\ \text{nm}}\right)^{-p}. \tag{4}$$

We have found that this leads to an improved match with experimental data and more realistic skin values as opposed to the approach where $\mu_s'(\lambda)$ is fixed according to average data from the literature [7]. The scattering properties of dermis are namely known to vary, tentatively with a person's age, gender, anatomical location, etc.

Because the literature data on scattering properties of the epidermis are very sparse and inconsistent [16], we apply the same ansatz also for the epidermis, but with two times higher amplitude a [7]. Similarly, the amplitude of scattering in subcutaneous adipose tissue (A) is also fitted individually, using a different ansatz [18], while its absorption spectrum is adopted from the literature [19]. The refractive index is set to $n = 1.45$ for the epidermis, 1.37 for dermis, and 1.34 for subcutis.

The best match with the experimental data is thus sought by varying 10 skin model parameters: the epidermal and dermal thickness (d_{epi} and d_{der}), epidermal melanin content (m), papillary and reticular dermal blood contents (b_{pap}, b_{der}), papillary and reticular blood oxygenation levels (S_{pap}, S_{ret}), dermal scattering amplitude and power (a, p), and scattering amplitude in the subcutis (A). Based on extensive preliminary testing, the thickness of the papillary dermis is fixed at 0.100 mm to improve the robustness of the inverse analysis.

Light transport and energy deposition in skin during the PPTR measurements are simulated using the established weighted-photon Monte Carlo (MC) technique [20]. The energy of the 532 nm laser pulse is divided into 10^7 energy packets ("photons") and their quasi-random tortuous paths through the scattering medium are followed until they deposit all the initial energy or escape through the skin surface. Due to the large computational complexity, this process is massively parallelized using CUDA technology (compute unified device architecture).

By considering also the thermal properties of the involved skin layers, the obtained laser-induced energy deposition profiles are then converted into the corresponding temperature profiles. And from these, the consequent PPTR signals are computed by accounting for partial absorption of the mid-IR emission contributions from subsurface tissue layers [3,4]. The initial 1.5 s of the PPTR signals are used in the analysis [see Fig. 3(a)].

The DRS spectra are simulated using the same MC algorithm. However, in order to control the computational load, the diffuse reflectance values are fitted at just 13 wavelengths, between 410 and 600 nm, and are carefully selected by considering specific features in the absorption spectra of melanin, oxyhemoglobin, and deoxyhemoglobin [see the arrows in Fig. 3(b)] [15].

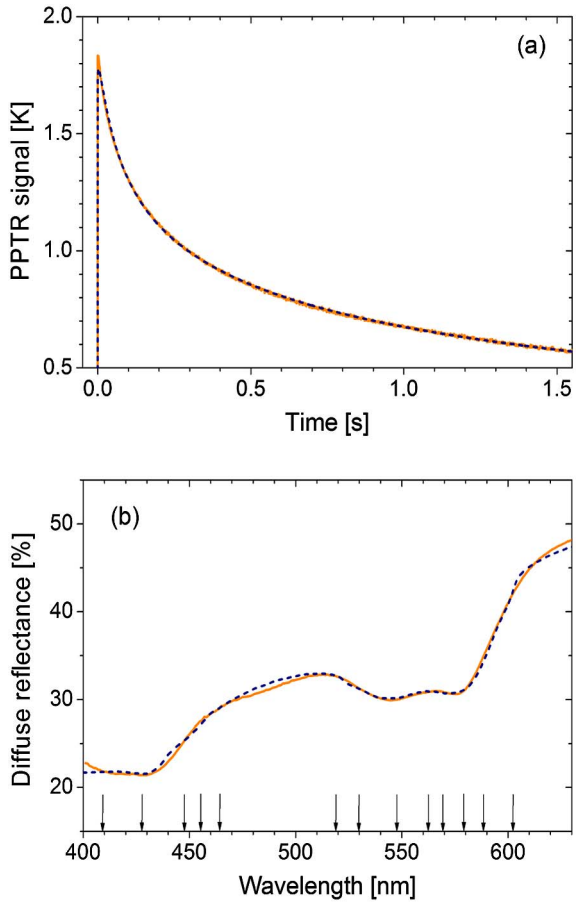

Fig. 3. (a) PPTR signal following pulsed irradiation at 532 nm and (b) DRS spectrum in the visible as measured in the forearm of a volunteer with healthy skin. Solid lines are experimental data (orange); dashed lines show best-fitting predictions of our numerical model.

The optimization problem is typically solved in 20–30 iterations, which takes 45–60 min on a reasonably powerful personal computer (Intel i7 processor, 16 GB of RAM) equipped with a high-performance graphics card (NVidia GTX 1070).

D. MPM

In order to enable a quantitative comparison with the above-presented approach, the same test sites were subsequently also imaged using an MPM system (MPTflex by JenLab, Jena, Germany) [12,13]. The instrument was approved for clinical research by the Institutional Review Board at the University of California at Irvine, U.S.

The instrument employs laser-scanning microscopy with optical contrast derived from TPEF of tissue components such as the cellular cofactors reduced nicotinamide adenine dinucleotide (NADH) and flavin adenine dinucleotide (FAD+), keratin, melanin, and elastin, as opposed to SHG, which occurs almost exclusively in dermal collagen fibers. We used the vertical scanning (x–z) operation mode, which provides cross-sectional images of the top part of skin *in vivo*.

A typical image of this kind (a.k.a. *b-scan*) with 1024 pixels × 1024 pixels is acquired in ~30 s. Four images

per test site, each translated relative to the previous one by a small distance in the direction perpendicular to the imaging plane, were acquired and saved for subsequent analysis.

3. RESULTS

A. From Combined PPTR and DRS

Figure 3 presents the PPTR signal transient (a) and diffuse reflectance spectrum (b) as measured on the volunteer's forearm (orange solid line). We can see that our optical-thermal model provides an excellent match between the experimental data and best-fitting model predictions (dashed line) for both included techniques. The small overshoot in the model DRS spectra at 470–510 nm is attributed to to the presence of skin chromophores such as beta-carotene and bilirubin, which are of no interest in the present study and were thus not included in the applied optical model.

The assessed skin parameter values for both test sites are presented in Table 1 in terms of average results and standard deviations from five analysis runs. (In the interest of clarity, the latter are omitted when smaller than 0.5 points on the last included decimal place).

All values lie within anatomically and physiologically plausible ranges for human skin, in accordance with our previous results from other volunteers and anatomical sites [7–9]. For example, the melanin fraction volume values (m) fall within the range of 1.3%–1.9%, reported earlier for fair Caucasian skin [21]. Using such values also produced realistic predictions of thermal injury thresholds in numerical modeling of pulsed laser irradiation of vascular lesions in human skin [15]. In addition, it is plausible (and rather convincing to see) that the assessed melanin fractional content is significantly larger in the more sun-exposed forearm ($m = 1.8$) as compared to the upper arm (1.3).

The blood volume fractions (between 1.6% and 2.6%) and oxygenation levels (44%–82%) are also very reasonable values, and the scattering parameters a and p are both within the respective ranges from the literature [7,16].

Similarly, both ET values (d_{epi}) lie between the minimal and maximal values as determined using the gold-standard cryohistology technique (30 and 175 μm, respectively, for the forearm) [22]. However, they are also significantly larger than the *mean* ET values as assessed more recently for the same anatomical site using the same technique (ET = 75 ± 13 μm) [11]. Practically the same result (ET = 72 ± 10 μm for the forearm in 20–40-year-old volunteers) was reported also in a systematic study using high-performance optical coherence tomography (OCT) [23].

In order to interpret the difference between our results (d_{epi}) and mean ET values from the literature, quoted above [11,23], it is essential to realize that the latter were determined from measurements of the ET in just five predefined locations within each cross-sectional image. Due to the strongly undulating nature of the epidermal-dermal junction and relative sparsity of the epidermal projections into papillary dermis (rete ridges), this makes it easy to miss the big picture of the epidermal anatomy. As a matter of fact, a closer inspection of the histology example presented in Ref. [23] (Fig. 1) reveals that the maximal ET in the presented field of view is around 0.10 mm, while the mean ET was assessed as 72 μm.

In contrast with the above, it seems plausible that our dual-modality analysis will likely sense the *maximal* ET, or an effective value strongly biased in this direction. Its determination is namely based on the sensitivity of DRS to specific spectral signature of the melanin in contrast with hemoglobin species present in the dermis. In addition, both PPTR and DRS signals are collected from relatively large surface areas, so the epidermal ridges are unlikely to be missed.

Table 1. Assessed Values of Our Skin Model Parameters (for Definitions See Section 2.C)[a]

Skin Property	Forearm	Upper Arm
d_{epi} [mm]	0.10	0.11
m [%]	1.8	1.3
b_{pap} [%]	1.6 ± 0.3	1.6 ± 0.1
b_{ret} [%]	2.6 ± 0.5	1.9 ± 0.2
S_{pap} [%]	82 ± 8	82 ± 7
S_{ret} [%]	44 ± 5	80 ± 3
a [mm^{-1}]	5.5 ± 0.2	4.7 ± 0.2
p [–]	1.5 ± 0.1	2.1 ± 0.2
d_{der} [mm]	0.79 ± 0.12	0.67 ± 0.03
A [–]	0.5 ± 0.1	1.6 ± 0.2

[a]Average results from five inverse analysis runs and the corresponding standard deviations (where significant) are presented.

B. MPM Cross-Sectional Images

In Fig. 4, we present cross-sectional images of the same skin sites as analyzed above, acquired using the MPM system. Owing to the good contrast between the TPEF signal from biomolecules that reside primarily in the highly cellular epidermis (presented in green), and the SHG signal (blue) originating

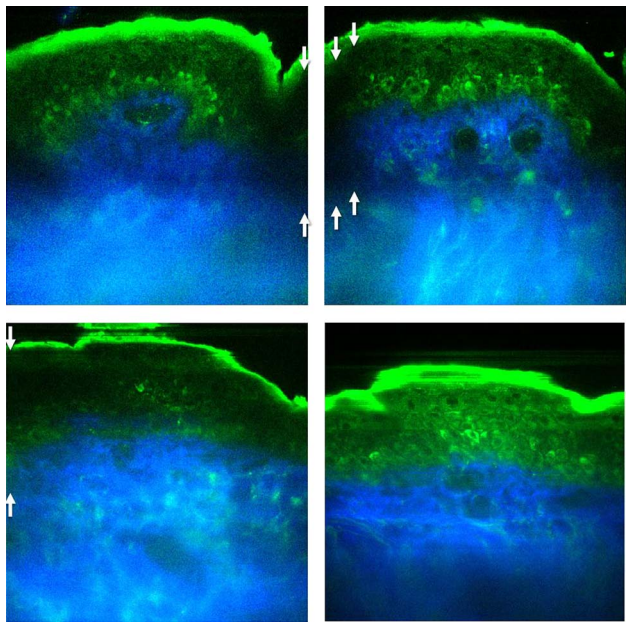

Fig. 4. Cross-sectional images of the same test sites obtained using MPM (top row, forearm; bottom, upper arm). The TPEF signal (green) arises from biomolecules that reside primarily in the epidermis, while SHG (blue) originates from collagen fibers in the dermis. The locations with maximal ET for each site are indicated with white arrows; the field of view is 0.20 mm. × 0.20 mm.

almost exclusively from collagen fibers in the underlying dermis, the epidermal-dermal junction can be identified quite easily.

It is notable that strong absorption and scattering in the epidermis attenuate considerably the TPEF signal from its deepest parts, i.e., the aforementioned rete ridges. This is why we consider also the dark columnar features present in some images in our assessment of the maximal ET (see white arrows in Fig. 4). Although very little TPEF signal is collected from these regions, the absence of SHG signal—indicative of dermal collagen and evidently present in other lateral locations at the same and even larger depths—strongly suggests that this is indeed an epidermal ridge.

In the presented images, we have accounted for the difference between the refractive indices of imaged skin and immersion medium, in which the MPM objective is moving to perform axial scanning (Immersol 518 F, by Carl Zeiss Inc; $n_{\mathrm{imm}} = 1.52$). In order to enable undistorted representation of the epidermal structure (keratinocytes and melanocytes) and more accurate assessment of the ET, the vertical scale was thus shrunk with respect to preprocessed images, according to the ratio $n_{\mathrm{epi}}/n_{\mathrm{imm}} = 0.96$.

By analyzing all acquired MPM images, we can thus estimate the maximal ET at both test locations to 0.10 mm. This is in very good agreement with values of d_{epi} in Table 1 and so provides support for our dual-modality analysis. At the same time, the presented comparison strongly supports our expectation that the analysis based on PPTR and DRS reports ET values that are closer to the maximal depth in a given anatomical location, rather than the somewhat artificially defined mean ET, which is currently more common in the literature.

4. DISCUSSION

The presented coregistration example, involving cross-sectional imaging using the MPM system, has provided us with first objective (albeit only partial) support for the innovative dual-modality analysis of skin structure and composition based on combined PPTR and DRS. Providing a definitive quantitative verification will evidently be very challenging, since there is, to the best of our knowledge, no established technique that would provide simultaneous assessment of the exact same set of skin properties *in vivo*.

In addition, the same comparison has provided a unique insight in terms of interpretation of the assessed d_{epi} values as near-maximal (rather than mean) ET values.

Admittedly, the MPM might not be the optimal approach for determination of the maximal ET. In addition to the strong reduction of the SHG and TPEF signal with depth, an important limitation is its narrow field of view (typically around 0.20 mm in the x direction), which makes it likely to miss the relatively sparse rete ridges. This could lead to incomplete understanding of the epidermal architecture and underestimation of the maximal ET.

The above limitation is further augmented by the shallow depth of field (in the y direction), which is, on the other hand, imperative for sharp high-resolution cross-sectional imaging, which is of course the main purpose and advantage of this instrument.

The above-stated benefits might thus be gained also using OCT, but this would require a suitable (e.g., 1300 nm wavelength) and high-resolution system. In one such study, for example, the authors reported that the range of ET values observed over all anatomic sites was smaller than the theoretical depth resolution (7.4 mm) of their OCT system [23].

Finally, while this report addresses primarily the assessment of ET, this is of course not the main purpose or even the point of skin characterization by combined PPTR and DRS. Quite to the contrary, there are obviously several more accurate, robust, and practical techniques available for this task in addition to OCT and MPM; high-frequency ultrasound, confocal microscopy, and photoacoustics, etc. are also available.

Admittedly, the computational complexity of the involved inverse analysis makes the presented dual-modality approach rather impractical and thus unsuitable for clinical deployment—at least using the currently applied hardware and mathematical algorithms. Nevertheless, its unique capability to assess many skin properties in parallel from quick and simple measurements utilizing relatively affordable equipment, constitutes a unique and attractive research technique that deserves further testing and development. The described advantages and positive preliminary tests have encouraged us to apply this technique in several innovative projects. These include a study of hemodynamics in self-healing bruises [5,9], where the presented approach is expanded by considering spatial diffusion of released hemoglobin and its breakdown products with specific spectral features. Another study in progressis exploring the potential to noninvasively sense collagen restructuring in fractional laser remodeling by means of sensitivity to dermal scattering properties (parameters a and p) [10].

5. CONCLUSIONS

Combining PPTR and DRS with inverse analysis based on numerical modeling (MC) of light transport in strongly scattering tissues enables noninvasive characterization of human skin in terms of the epidermal and dermal thickness, specific chromophore contents, and scattering properties. The assessed ET values (d_{epi}) were compared with high-resolution cross-sectional images, acquired from two test sites in a human volunteer using MPM. The results show that d_{epi} values correspond very well to the maximal ETs measured in the MPM images, corresponding to the epidermal projections into papillary dermis (rete ridges).

Funding. Javna Agencija za Raziskovalno Dejavnost RS (ARRS) (BI-US 16-17-059, P1-0192, PR-07590); National Institute of Biomedical Imaging and Bioengineering (NIBIB) (P41EB015890).

Acknowledgment. We thank Fotona d.o.o. (Ljubljana, Slovenia) and JenLab GmbH (Jena, Germany) for lending us the medical laser system for PPTR and MPM measurements, respectively. A part of this work was presented at the 14th International Workshop on Advanced Infrared Technology and Applications, AITA 2017 [6].

REFERENCES

1. T. E. Milner, D. M. Goodman, B. S. Tanenbaum, and J. S. Nelson, "Depth profiling of laser-heated chromophores in biological tissues by pulsed photothermal radiometry," J. Opt. Soc. Am. A **12**, 1479–1488 (1995).
2. B. Majaron, W. Verkruysse, B. S. Tanenbaum, T. E. Milner, S. A. Telenkov, D. M. Goodman, and J. S. Nelson, "Combining two excitation wavelengths for pulsed photothermal profiling of hypervascular lesions in human skin," Phys. Med. Biol. **45**, 1913–1922 (2000).
3. M. Milanič, I. Serša, and B. Majaron, "A spectrally composite reconstruction approach for improved resolution of pulsed photothermal temperature profiling in water-based samples," Phys. Med. Biol. **54**, 2829–2844 (2009).
4. L. Vidovič, M. Milanič, and B. Majaron, "Objective characterization of bruise evolution using photothermal depth profiling and Monte Carlo modeling," J. Biomed. Opt. **20**, 017001 (2015).
5. L. Vidovič, M. Milanič, L. L. Randeberg, and B. Majaron, "Quantitative characterization of traumatic bruises by combined pulsed photothermal radiometry and diffuse reflectance spectroscopy," Proc. SPIE **9303**, 930307 (2015).
6. B. Majaron, N. Verdel, A. Marin, L. Vidovič, and M. Milanič, "Quantitative characterization of human skin by combined photothermal radiometry and optical spectroscopy," in *14th International Workshop on Advanced Infrared Technology and Applications, AITA* (2017), pp. 35–38.
7. N. Verdel, A. Marin, L. Vidovič, M. Milanič, and B. Majaron, "In vivo characterization of structural and optical properties of human skin by combined photothermal radiometry and diffuse reflectance spectroscopy," Proc. SPIE **10037**, 100370H (2017).
8. N. Verdel, A. Marin, L. Vidovič, M. Milanič, and B. Majaron, "Analysis of hemodynamics in human skin using photothermal radiometry and diffuse reflectance spectroscopy," Proc. SPIE **10413**, 104130O (2017).
9. A. Marin, N. Verdel, L. Vidovič, M. Milanič, and B. Majaron, "Assessment of individual bruising dynamics by pulsed photothermal radiometry and inverse Monte Carlo analysis," Proc. SPIE **10413**, 104130P (2017).
10. N. Verdel, A. Marin, M. Lukač, and B. Majaron, "Noninvasive assessment of changes in human skin upon fractional laser remodeling," Lasers Surg. Med. **50**, S5 (2018).
11. J. Sandby-Moller, T. Poulsen, and H. C. Wulf, "Epidermal thickness at different body sites: relationship to age, gender, pigmentation, blood content, skin type and smoking habits," Acta Derm. Venereol. **83**, 410–413 (2003).
12. M. Weinigel, H. G. Breunig, A. Gregory, P. Fischer, M. Kellner-Höfer, R. Bückle, and K. König, "A novel flexible clinical multiphoton tomograph for early melanoma detection, skin analysis, testing of anti-age products, and in situ nanoparticle tracking," Proc. SPIE **7589**, 758908 (2010).
13. M. Balu, C. B. Zachary, R. M. Harris, T. B. Krasieva, K. König, B. J. Tromberg, and K. M. Kelly, "In vivo multiphoton microscopy of basal cell carcinoma," JAMA Dermatol. **151**, 1068–1074 (2015).
14. L. Vidovič and B. Majaron, "Elimination of single-beam substitution error in diffuse reflectance measurements using an integrating sphere," J. Biomed. Opt. **19**, 027006 (2014).
15. M. Milanič and B. Majaron, "Three-dimensional Monte Carlo model of pulsed-laser treatment of cutaneous vascular lesions," J. Biomed. Opt. **16**, 128002 (2011).
16. S. L. Jacques, "Optical properties of biological tissues: a review," Phys. Med. Biol. **58**, 5007–5008 (2013).
17. M. Friebel, A. Roggan, G. Müller, and M. Meinke, "Determination of optical properties of human blood in the spectral range 250 to 1100 nm using Monte Carlo simulations with hematocrit-dependent effective scattering phase functions," J. Biomed. Opt. **11**, 034021 (2006).
18. P. Naglič, L. Vidovič, M. Milanič, L. L. Randeberg, and B. Majaron, "Applicability of diffusion approximation in analysis of diffuse reflectance spectra from healthy human skin," Proc. SPIE **9032**, 90320N (2013).
19. C. R. Simpson, M. Kohl, M. Essenpreis, and M. Cope, "Near-infrared optical properties of *ex vivo* human skin and subcutaneous tissues measured using the Monte Carlo inversion technique," Phys. Med. Biol. **43**, 2465–2478 (1998).
20. L. Wang, S. L. Jacques, and L. Zheng, "MCML-Monte Carlo modeling of light transport in multi-layered tissues," Comput. Methods Programs Biomed. **47**, 131–146 (1995).
21. L. Svaasand, L. Norvang, E. Fiskerstrand, E. Stopps, M. Berns, and J. Nelson, "Tissue parameters determining the visual appearance of normal skin and port-wine stains," Laser Med. Sci. **10**, 55–65 (1995).
22. R. C. Hermann, C. N. Ellis, D. W. Fitting, V. C. Ho, and J. J. Voorhees, "Measurement of epidermal thickness in normal skin and psoriasis with high-frequency ultrasound," Skin Pharmacol. Physiol. **1**, 128–136 (1988).
23. T. Gambichler, R. Matip, G. Moussa, P. Altmeyer, and K. Hoffmann, "In vivo data of epidermal thickness evaluated by optical coherence tomography: effects of age, gender, skin type, and anatomic site," J. Dermatol. Sci. **44**, 145–152 (2006).